Basic principles of acoustic emission tomography

Dr. Frank Schubert
Fraunhofer-Institute for Nondestructive Testing (IZFP)
Branch Lab EADQ, Dresden, Germany

Abstract

The present paper describes the basic principles of acoustic emission tomography. This method uses acoustic emission events as point sources and combines the usual iterative localisation algorithm of acoustic emission testing with algorithms for travel time tomography like ART (algebraic reconstruction technique). The procedure is equivalent to the solution of the generalised inverse localisation problem in locally isotropic heterogeneous media and leads to a new imaging technique where in addition to the source positions the volume of the specimen is visualised in terms of a locally varying wave speed distribution. It is shown by numerically obtained data sets that the algorithm leads to a more accurate localisation of acoustic emission events and offers totally new perspectives for acoustic emission imaging and for acoustic tomography in general.

1. Introduction and outline

Localisation algorithms in acoustic emission (AE) testing mostly use the assumption of a homogeneous background medium with constant wave speed in order to determine the location of acoustic emission events. However in practice, the structures under investigation are inhomogeneous in many cases, i.e. wave speeds are changing in space and time due to heterogeneities of the microstructure (e.g. grains and pores), the effect of structural components (e.g. tendon ducts in concrete), and material changes caused by the damage mechanism itself (e.g. crack growth). These heterogeneities limit the accuracy of source localisation algorithms.

In order to overcome these drawbacks the usual localisation algorithm of acoustic emission testing can be combined with travel time tomography by using the AE events as acoustic point sources. In this context a re-localisation, i.e. an update of the current source positions, has to be performed after each tomographic inversion resulting in an iterative procedure with alternating steps of source localisation and tomography. This method is in principle known from geophysics where earthquakes are located and used for tomographic imaging of the earth's interior.

Chapter 2 first summarises the fundamentals of iterative AE localisation and describes how the underlying equations can simply be generalised to heterogeneous media. Chapter 3 briefly describes the different approaches of tomographic imaging with diffracting and non-diffracting sources paying particular attention to algebraic reconstruction techniques (ART). Chapter 4 shows how the two concepts of localisation and travel-time tomography can be combined resulting in an iterative algorithm for acoustic emission tomography called AE-TOMO. In chapter 5 numerical AE data obtained by the elastodynamic finite integration technique (EFIT) are used to demonstrate the physical soundness of the proposed method. It is further shown that the AE-TOMO approach offers totally new perspectives, not only for acoustic emission imaging but also for traditional acoustic tomography since AE events can also be produced artificially at the outer surfaces of the specimen under investigation (e.g. by pencil lead breaks or hammer impacts). Finally an outlook is given how the present algorithms could be improved by using further advanced tomographic imaging techniques and how acoustic emission tomography can be verified experimentally.

2. Source localisation

Let us suppose we have $i = 1,...,N$ sensors and the P-wave arrival times of a single acoustic emission event have been determined by using an appropriate picking algorithm. In a first approximation the arrival time at sensor i is given by

$$t_i^A = \frac{\left| \underline{r}_i^S - \underline{r} \right|}{c_i} + t = \frac{\sqrt{\left(x_i^S - x\right)^2 + \left(y_i^S - y\right)^2 + \left(z_i^S - z\right)^2}}{c_i} + t \quad , \tag{1}$$

where $\underline{r}_i^S = (x_i^S, y_i^S, z_i^S)$ is the known position of sensor i and $\underline{r} = (x, y, z)$ is the unknown location of the AE event to be determined by the localisation algorithm. t represents the source time of the AE event and is usually measured relative to a trigger level.

Eq. (1) is based on a simple straight ray model regarding the source-sensor travel path. In this context c_i is the mean effective wave speed along ray i. In most cases, AE localisation is done under the assumption of a homogeneous background medium and thus, $c_i = c = constant$ for all rays, $i = 1,...,N$. On the other hand, in a heterogeneous medium the effective wave speed can be different from one ray to another, i.e. $c_i \neq c_j$ for $i \neq j$, in general.

In Eq. (1) we have four unknowns, namely the three source coordinates x, y, z and the source time t. Thus, at least four different sensor arrival times are needed to solve the underlying system of equations. Since Eq. (1) represents a nonlinear system of equations, a closed analytical solution is not available in general and thus, it has to be solved by an iterative method.

For that purpose we start with some initial values x_0, y_0, z_0, t_0 and suppose that the effective wave speeds c_i are all known. By using the same straight ray model as explained above we can now calculate the theoretical arrival times $t_{i,0}^A$ using Eq. (1). In general, these theoretical times will be different from the measured arrival times, T_i^A. From the differences $\Delta t_i^A = T_i^A - t_{i,0}^A$, the correction values for the next iteration $\Delta x, \Delta y, \Delta z, \Delta t$ can be obtained. Since the measured arrival times can be written as a function of $x, y, z,$ and t,

$$T_i^A = f_i(x, y, z, t) = t_{i,0}^A + \Delta t_i^A = t_{i,0}^A + \frac{\partial f_i}{\partial x} \Delta x + \frac{\partial f_i}{\partial y} \Delta y + \frac{\partial f_i}{\partial z} \Delta z + \frac{\partial f_i}{\partial t} \Delta t \quad , \tag{2}$$

the arrival time difference Δt_i^A is expressed as total differential of f_i. In matrix form we have

$$\begin{pmatrix} \Delta t_1^A \\ . \\ . \\ . \\ . \\ \Delta t_N^A \end{pmatrix} = \begin{pmatrix} \frac{\partial f_1}{\partial x} & \frac{\partial f_1}{\partial y} & \frac{\partial f_1}{\partial z} & \frac{\partial f_1}{\partial t} \\ . & . & . & . \\ . & . & . & . \\ . & . & . & . \\ \frac{\partial f_N}{\partial x} & \frac{\partial f_N}{\partial y} & \frac{\partial f_N}{\partial z} & \frac{\partial f_N}{\partial t} \end{pmatrix} \cdot \begin{pmatrix} \Delta x \\ \Delta y \\ \Delta z \\ \Delta t \end{pmatrix} \quad , \tag{3}$$

or shortly,

$$\underline{\Delta t}^A = \underline{\underline{F}} \cdot \underline{\Delta s} \quad , \tag{4}$$

where $\underline{\Delta t}^A$ and $\underline{\underline{F}}$ are known while $\underline{\Delta s}$ is unknown. If the number of sensors is $N = 4$, the solution of Eq. (4) is well-defined, namely

$$\underline{\Delta s} = \underline{\underline{F}}^{-1} \cdot \underline{\Delta t}^A \quad . \tag{5}$$

If N > 4, the problem is over-determined. In this case a least-square approximation with regard to arrival time differences is given by the normal equation,

$$\underline{\Delta s} = \left(\underline{\underline{F}}^T \cdot \underline{\underline{F}}\right)^{-1} \cdot \underline{\underline{F}}^T \cdot \underline{\Delta t}^A \qquad . \tag{6}$$

Using the result of Eq. (6), the update of source coordinates and source time from iteration 0 to iteration 1, or more general from iteration k to $k+1$ can now be expressed as

$$\begin{aligned}
x^{(k+1)} &= x^{(k)} + R_x \Delta x \\
y^{(k+1)} &= y^{(k)} + R_y \Delta y \\
z^{(k+1)} &= z^{(k)} + R_z \Delta z \\
t^{(k+1)} &= t^{(k)} + R_t \Delta t
\end{aligned} \qquad , \tag{7}$$

where the R_j's with $0 \leq R_j \leq 1$ and $j = x, y, z, t$ are relaxation parameters. In order to ensure convergence of the iterative method, values of $R \approx 0.1$ are typically used.

3. Acoustic tomography

In acoustic tomography, data collected from sending acoustic waves through an object at many different angles are used to compute an image of changes of a physical quantity within the object under investigation (e.g. attenuation or wave speed in transmission tomography or acoustic impedance mismatch in reflection tomography). In traditional acoustic tomography the sound waves are passed from a series of sources to receivers at various locations around the specimen (Fig. 1).
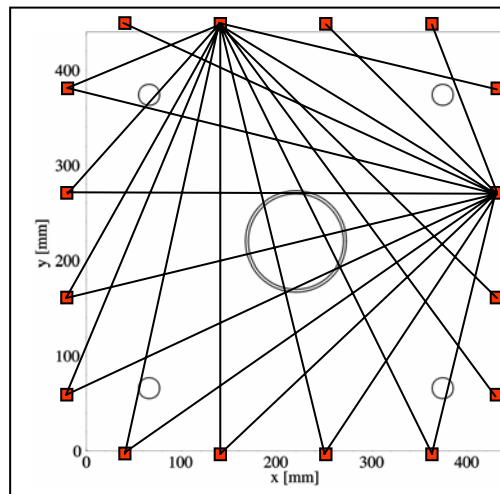

Figure 1: Source/receiver geometry for traditional acoustic tomography. A number of transducers (actuators and/or receivers) is located at the outer surfaces of the specimen. In order to ensure a high depth of ray coverage, a large number of evenly distributed transducers is necessary. If the number of transducers is N, at most N² ray paths can be used for tomographic imaging (exact number depends on transducer configuration and operation mode (reflection or transmission)).

Usually each transducer is used as both, source and receiver, resulting in at most N^2 ray paths if the number of transducers is N. For example, the travel times between each source and receiver are measured. In this case the resulting tomographic images represent the locally vary-

ing wave speed distribution inside the specimen. Alternatively, the amplitudes of the transmitted time-domain signals at the receivers can be measured and the variations in attenuation may be reconstructed. The latter method, however, makes high demands on the transducer coupling conditions. Another possibility is the measurement of reflected signals and the reconstruction of the acoustic impedance mismatch between matrix and scatterers ("reflection tomography").

Mathematically, there are two major classes of tomographic reconstruction techniques [1]. One class, the transform based methods are using the Fourier-slice theorem for non-diffracting sources and the Fourier-diffraction theorem for diffracting sources, respectively. These methods are fast but have the restriction that the data must be acquired on evenly spaced sets of straight rays ("projections").

A second type of methods employs iterative procedures to reconstruct an image. The most widely used of these methods is called algebraic reconstruction technique (ART). Other related iterative techniques are SIRT (simultaneous iterative reconstruction technique) and SART (simultaneous algebraic reconstruction technique). These techniques are less efficient than transform based methods but they have several advantages. They can be used with irregular sampling geometries, incomplete data sets, and may incorporate curved ray paths. In recent years powerful ray tracing algorithms have been developed correcting for both, diffraction and refraction of the wave field. In the present paper, a transmission ART algorithm with straight ray paths has been used in a first step due to its simplicity and its potential for further ray tracing enhancements as mentioned above. This implies by no means that ART represents the best method for the problem described in this paper.

The ART algorithm adjusts the estimated slowness values, $s_{ij} = 1/c_{ij}$, of the discrete tomography cells (i,j) in a systematic fashion until the computed arrival times, t_p^A, for ray p ($p = 1,...,N_p$) match the measured arrival times, T_p^A. For that purpose, the path lengths, l_{ij}^p, of each ray p in tomography cell (i,j) and the computed arrival times for iteration k are used to obtain a new estimate of the slowness for iteration $k+1$:

$$s_{ij}^{(k+1)} = s_{ij}^{(k)} + R \cdot \Delta s_{ij} \quad , \tag{8}$$

with

$$\Delta s_{ij} = (T_p^A - t_p^A) \frac{l_{ij}^p}{\sum_{i,j} (l_{ij}^p)^2} \quad , \tag{9}$$

and

$$t_p^A = \sum_{i,j} s_{ij}^{(k)} l_{ij}^p \quad . \tag{10}$$

The summation in Eqs. (9) and (10) is performed over all tomography cells (i,j) passed by ray p. R is a relaxation parameter used to improve stability and convergence of the method. Small values of R between 0.01 und 0.1 are typical and provide some filtering behaviour.

ART makes the slowness adjustment on a ray-by-ray basis [2]. In contrast to that, the SIRT method uses an average correction for all rays applied to each tomography cell [3], but was not employed here.

4. Acoustic emission tomography

With the basic principles described in the previous two chapters it is now very easy to depict the concept of acoustic emission tomography using AE events as tomographic sources (Fig. 2).
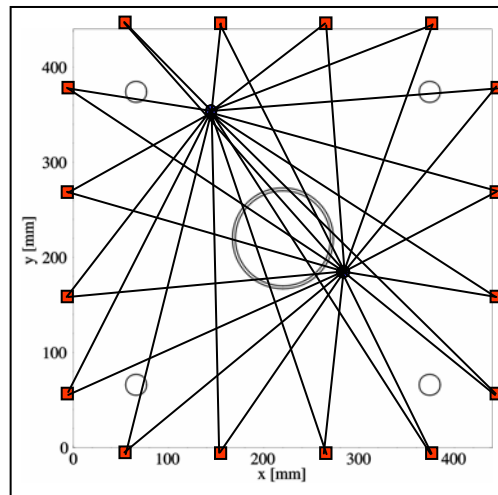
Figure 2: *Source/receiver geometry for acoustic emission tomography. The AE events inside the specimen are used as acoustic point sources. Only sensors are needed at the outer surfaces of the specimen. Naturally, a high depth of ray coverage is reached since the number of AE events typically lies in the range of some hundreds or thousands.*

We start with an initial guess of the slowness distribution, typically a homogeneous medium with constant wave speed (step 0). In step 1 we perform an initial localisation of the AE sources using the method described in chapter 2. The initial source locations are then used to perform an ART tomography as described in chapter 3 (step 2). The result is an updated heterogeneous model with locally varying slowness and wave speed, respectively.

This heterogeneous model can now be used to perform a re-localisation of the AE sources using different effective wave speeds for each ray (step 1 again). In a further step the modified and improved source positions permit an improved tomography result (step 2 again) which in turn leads to better source positions (step 1) and so on (step 2 ↔ step 1).

This iterative procedure is repeated until the squares of arrival time differences between measured and computed times (residues) reach a minimum or a predefined accuracy level. The procedure is equivalent to the solution of the generalized inverse localisation problem in locally isotropic heterogeneous media and leads to a new imaging technique where in addition to the source positions the volume of the specimen is visualised in terms of a locally varying wave speed distribution.

While in traditional acoustic tomography the number of available ray paths and thus, the depth of coverage is limited by the number of actuators and receivers, in AE tomography hundreds or thousands of AE events are typically available. Therefore, a relatively small number of sensors, e.g. *N = 8* or less, can be compensated by picking a correspondingly larger number of AE events. Of course, the locations of AE events are usually restricted to some active areas like damage zones leading to a more or less non-uniform coverage of rays. However, the large number of rays should also compensate for this inhomogeneity to some extent. Moreover, imaging of the immediate vicinity of damage zones is of high practical interest and in these zones, an extremely high depth of ray coverage and thus, a high spatial resolution of the tomographic image should be achievable.

Another important advantage of acoustic emission tomography compared to traditional acoustic emission testing is connected with the use of "unwanted" AE events. For example in an aircraft usually the majority of AE events is produced by sources of interference like joints and great effort is required to separate these unwanted signals from wanted signals generated by cracks or other defects. In AE tomography, these unwanted sources can also be used for tomographic imaging provided that they can also be treated as transient point sources. While traditional AE analysis provides information about the location of active AE regions, acoustic

emission tomography visualises both, active and non-active regions of the specimen. Therefore, acoustically "passive" defects in the structure can also be identified in principle.

The list of advantages of AE tomography as described above is by no means complete. Since acoustic emission events can also be produced artificially, e.g. by pencil lead breaks or hammer impacts at the surface of a specimen, new paradigms in acoustic NDT tomography in general are imaginable as explained in somewhat more detail in the outlook.

At the end of this chapter it is important to point out that acoustic emission tomography represents a purely algorithmic extension of traditional AE analysis using exactly the same raw data, i.e. no additional expenses concerning data acquisition are necessary in general.

5.   Acoustic emission tomography with numerical data

In order to demonstrate the physical soundness of acoustic emission tomography, numerical AE data sets calculated by the elastodynamic finite integration technique (EFIT, [4]) were used. For that purpose, the cross-section of an existing concrete specimen (440×440 mm²) with steel reinforcement and tendon duct was chosen (see Fig. 2 and [5]). The specimen was used for fatigue tests and was assigned for AE measurements as well.

The cross section in Fig. 2 shows four steel reinforcement bars with diameters of 22 mm in the corners ($c_P = 5900$ m/s, $c_S = 3200$ m/s, $\rho = 7820$ kg/m³) and an ungrouted polyethylene tendon duct with inner diameter of 100 mm and a wall thickness of 3 mm in the middle of the model ($c_P = 2300$ m/s, $c_S = 1200$ m/s, $\rho = 950$ kg/m³). 16 sensors were placed at the outer surfaces of the specimen using a distance of 11 cm to each other. In this first step the concrete matrix was approximated as homogeneous background medium ($c_P = 3950$ m/s, $c_S = 2250$ m/s, $\rho = 2050$ kg/m³), the sensors as point detectors. Moreover idealised isotropic AE sources were realised, generating P-waves only. As shown in [5] these simplifying assumptions can easily be dropped and more realistic models including aggregates, pores, grouted tendon ducts filled with mortar and steel strands as well as AE sources with more realistic crack mechanisms can be simulated in further investigations but are omitted here.

A total of 40 AE events with random locations inside the model (but restricted to the concrete matrix) were calculated. Fig. 3 exemplary shows the wave front snapshots of six AE events taken at a time of 25.3 µs after source excitation in each case. The pictures clearly show the interaction of the pressure waves with tendon duct, steel reinforcement, and outer surfaces of the specimen, respectively. The normal components of particle velocity were calculated at the individual sensor positions shown in Fig. 2. After that, the first-arrival times of the time-domain signals were determined by using an automated picking algorithm based on the Hinkley criterion [6]. These arrival times then served as input for the acoustic emission tomography algorithm called AE-TOMO.

The ray coverage due to the 40 AE sources is shown in Fig. 4. A total of $40 \times 16 = 640$ rays was used for AE tomography. Due to the random locations of the AE events a more or less uniform coverage of the model was reached. Only the corners are not covered. It can also be seen that the steel cable in the bottom left corner is worse covered than the remaining three cables due to a lower density of AE events in this region.

Since the locations of all AE events in the simulation are exactly known, the accuracy of the traditional localisation algorithm as described in chapter 2 can be evaluated and compared with the AE-TOMO algorithm. Since the traditional algorithm uses a homogeneous background medium, the results strongly depend on the chosen P-wave velocity of the matrix as shown in Fig. 5. In this case, a minimum source location error of ± 2 mm is reached at $c_P \approx$ 3930 m/s.
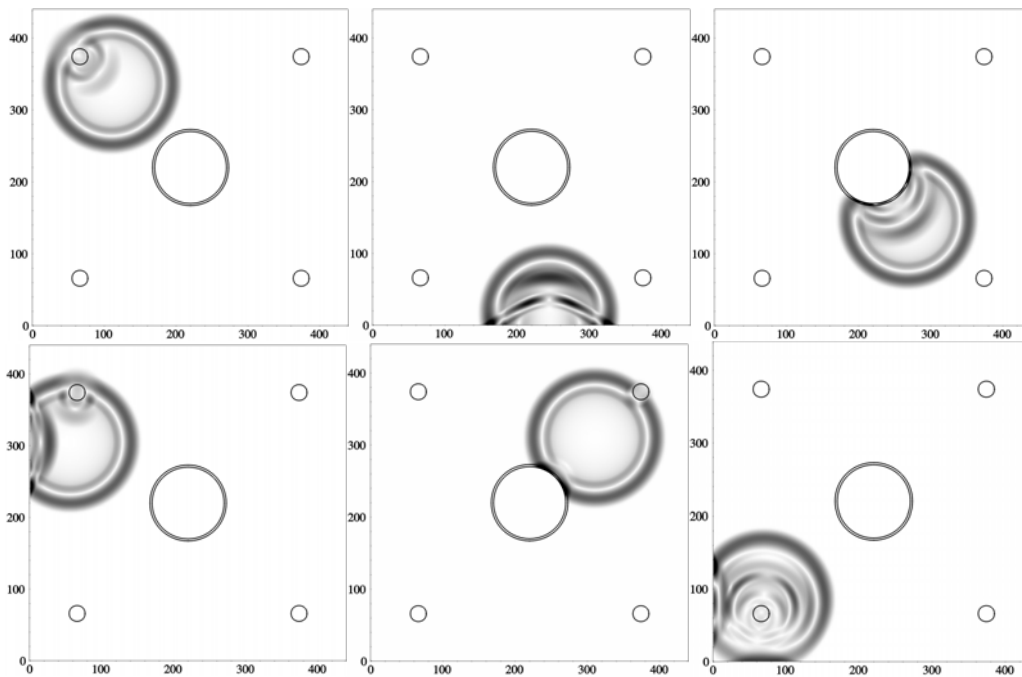
Figure 3: Wave front snapshots of six different acoustic emission events as calculated by the numerical EFIT code. The pictures represent the absolute value of particle velocity using a linear grey scale. They are taken at 25.3 µs after source excitation in each case. All in all, 40 AE events were calculated, analysed, and used for acoustic emission tomography.
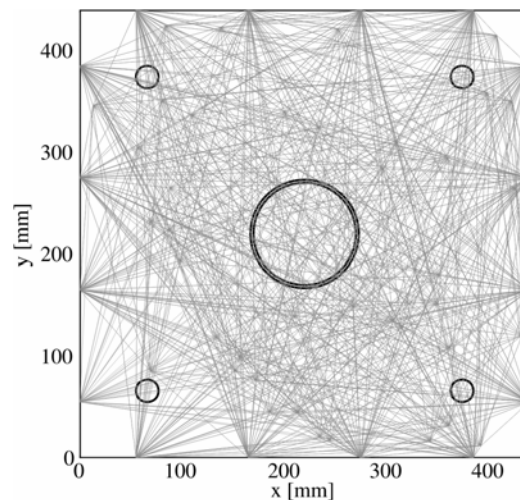

Figure 4: Ray coverage of the model according to 40 AE events and 16 sensors. Thus, a total of 640 rays were used for acoustic emission tomography. Due to the random locations of the AE events a more or less uniform coverage of the model is reached. Only the corners of the model are not covered.

If the mean effective wave speed varies in the range of a few percent – which is the typical inaccuracy in experimental measurements – the mean error of source location increases by a few hundred percent as can be seen in Fig. 5. In order to avoid this problem, the wave speed could be incorporated as a further unknown into the traditional localisation algorithm. However, our investigations revealed that in this case the minimum error of source location amounts to about ± 4.5 mm which is significantly larger than obtained by the normal localisation algorithm with constant wave speed (± 2 mm). Moreover, the enhanced algorithm turned out to be numerically less stable. The results of both localisation algorithms are summarised in Table 1 and compared with the results of acoustic emission tomography.
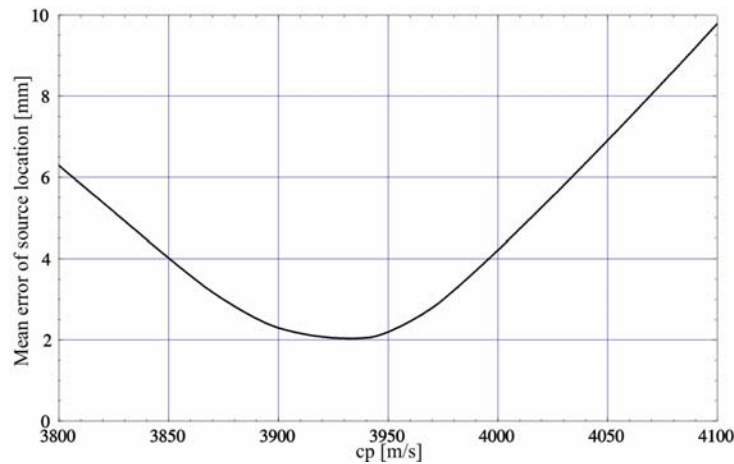
Figure 5: *Mean error of source location as a function of matrix wave speed as obtained by the traditional (normal) localisation algorithm. Deviations of only 3-4% in acoustic P-wave speed ($\approx 3930 \pm 150$ m/s) lead to an increase of source location error by 300-500% (from 2 mm at the minimum up to 6 and 10 mm, respectively).*

	Normal localisation (homogeneous matrix); Unknowns: x,y,(z),t	**Enhanced localisation** (homogeneous matrix); Unknowns : x,y,(z),t,c_P	**Acoustic emission tomography** (heterogeneous matrix); Unknowns: x,y,(z),t, $c_P(x,y,z)$
Mean residual	0.71 µs	0.72 µs	0.12 µs
Minimum residual	0.42 µs	0.42 µs	0.04 µs
Maximum residual	1.17 µs	1.14 µs	0.35 µs
Mean source location error	2.20 mm	4.54 mm	0.90 mm
Minimum source location error	0.31 mm	0.17 mm	0.10 mm
Maximum source location error	4.98 mm	10.0 mm	3.82 mm
Mean source time error	0.25 µs	1.41 µs	0.11 µs
Minimum source time error	0.04 µs	0.01 µs	0.001 µs
Maximum source time error	0.53 µs	4.25 µs	0.43 µs

Table 1: *Results for normal localisation, enhanced localisation, and acoustic emission tomography obtained at the model in Fig. 4 (40 AE events, 16 sensors). The results for AE tomography are significantly better than for the traditional algorithms since heterogeneity of the medium is taken into account. The spatial coordinate z is given in parentheses since the underlying problem is effectively 2-D. For the normal localisation the values at $c_P = 3950$ m/s are listed (compare Fig. 5).*

By using the AE-TOMO algorithm significantly better results for localisation are obtained than for the traditional algorithms since heterogeneity of the medium is taken into account. Moreover, each new AE event leads to a better approximation of the spatial velocity field and thus, also to a better localisation of the *preceding* AE events. Therefore, increasing the number of AE events in AE tomography improves the overall accuracy of localisation while traditional localisation of AE events is performed independently from each other, i.e. the mean error is more or less independent from the number of AE events.
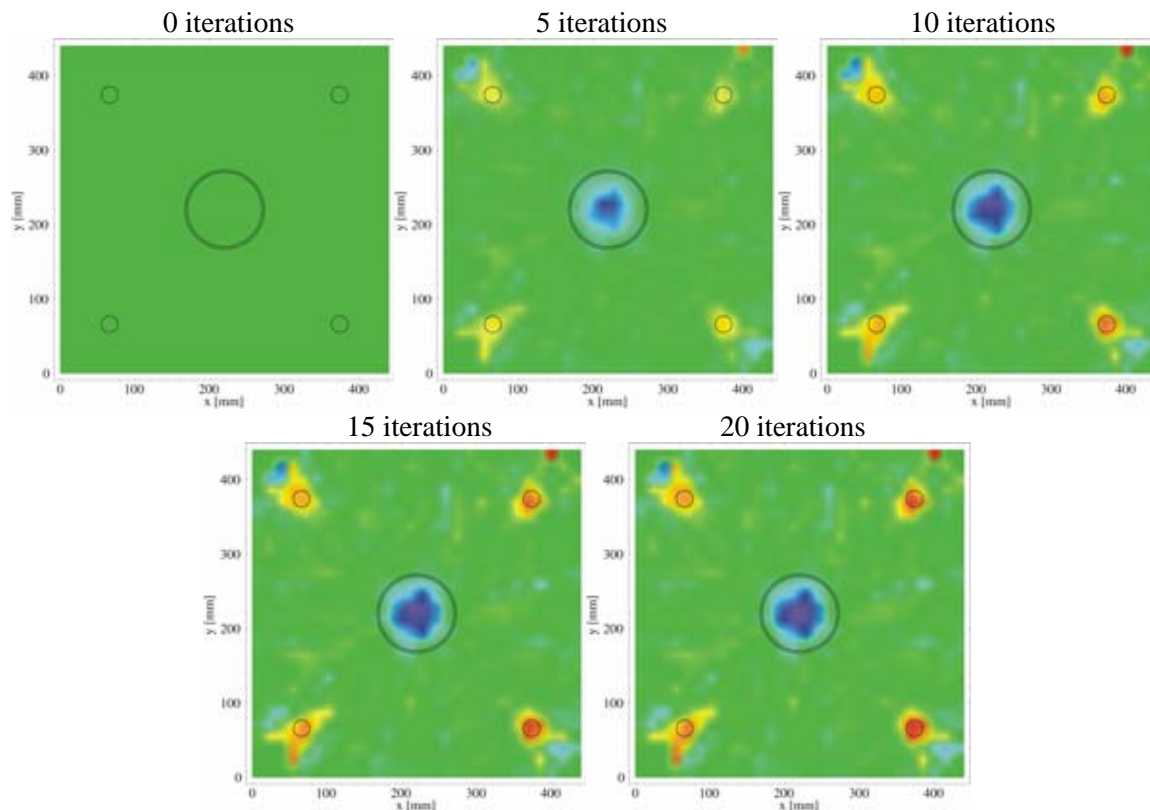
Figure 6: Tomographic images of the model after 0, 5, 10, 15, and 20 iterations of the AE-TOMO algorithm (28 × 28 pixels with anti-aliasing). After about 15 iterations the wave speed model becomes more and more stable. The steel cables with locally increased wave speed (red color) in the corners and the ungrouted tendon duct with decreased wave speed (blue color) in the middle of the model are clearly visible.

Fig. 6 shows tomographic images after 0 (homogeneous start model), 5, 10, 15, and 20 iterations of the AE-TOMO algorithm obtained at the model from Fig. 4 (40 AE events, 16 sensors). One can see that after about 10-15 iterations the wave speed model becomes more and more stable. The steel reinforcement cables with locally increased wave speed (red color) in the corners as well as the ungrouted tendon duct with effectively decreased wave speed (blue color) in the middle of the model are clearly visible. It is obvious that the reconstruction of the steel cable in the bottom left corner is worse than for the remaining three cables which is most likely caused by the worse ray coverage as shown in Fig. 4.

Fig. 7 shows the influence of the number of AE events on the tomography result (after 20 iterations in each case). The corresponding pictures represent the wave speed model using 5, 10, 20, 30, and 40 AE events for tomographic reconstruction. If the number of available sources and thus, the number of rays is increased the model becomes better and better. However, similar to Fig. 6 a saturation behavior can be observed if the ray coverage of the tomography cells reaches a certain level. A further increase of the number of rays would not automatically improve the quality of the image if we keep the number of tomography cells constant. Instead we could increase the number of cells and thus, the spatial resolution of the tomographic image. With typical numbers of AE events in the range of hundreds or thousands image resolutions that can never be reached with traditional acoustic tomography seem to be possible.
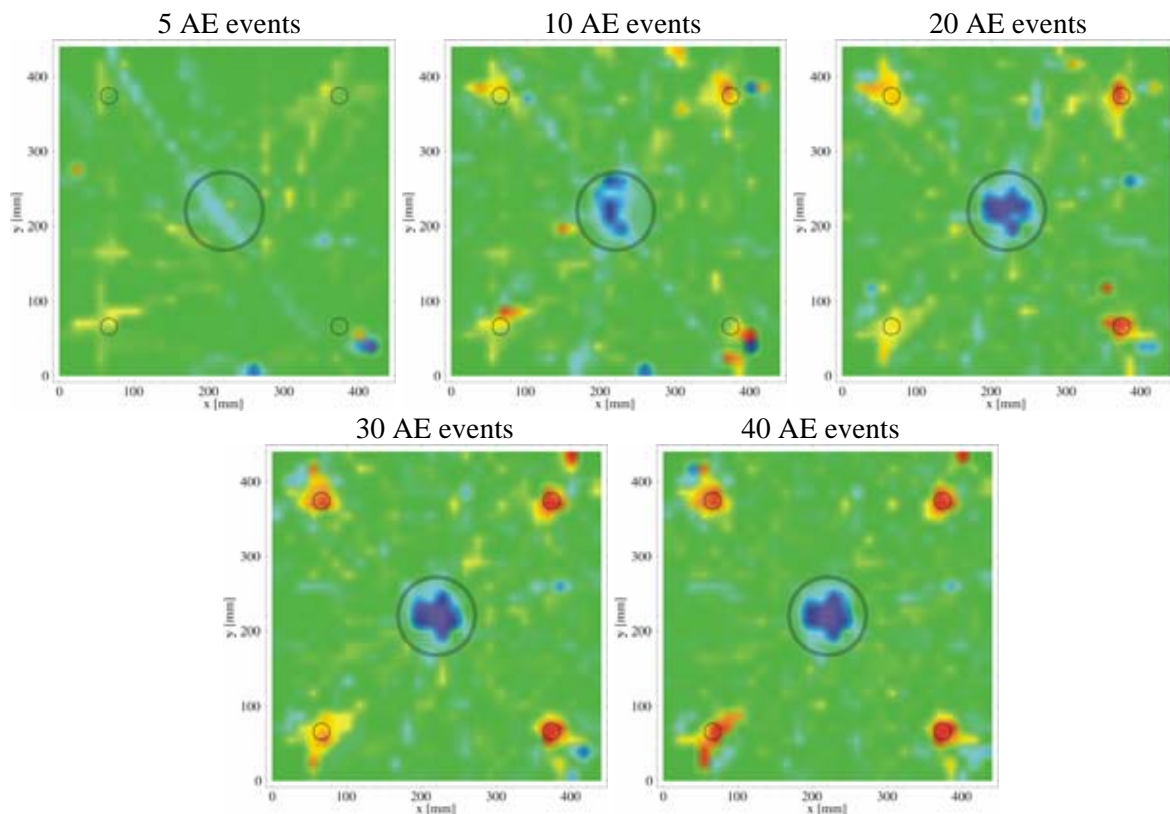
Figure 7: Tomographic images of the model using 5, 10, 20, 30, and 40 AE events for reconstruction (28 × 28 pixels with anti-aliasing). The wave speed model becomes better and better if the number of AE events and thus, the number of rays is increased.

However, as can be seen in Figs. 6 and 7 there are still some artefacts in the tomographic images most likely caused by the simple straight line approximation of the ray model. Due to the large differences in acoustic impedance between the matrix and the scatterers (steel reinforcement and ungrouted tendon duct, respectively) this straight line approximation is not sufficiently fulfilled in the present case. Thus, taking diffraction and refraction effects with curved ray paths into account should lead to significantly improved images in the future.

Another reason for some of the artefacts is the non-uniform ray coverage of the model leading to large differences in the number of rays passing through the equally sized tomography cells. As a consequence, working with adaptively sized tomography cells should lead to a more evenly ray density per cell and thus, to a better tomographic image.

6. Summary and outlook

In the present paper it has been shown that acoustic emission tomography represents an important improvement of traditional AE analysis leading to significantly better localisation of AE events due to consideration of heterogeneous media. The method leads to a new imaging technique where in addition to the source positions the volume of the specimen is visualised in terms of a locally varying wave speed distribution.

Apart from that, AE tomography has self-contained relevance since in the traditional sense "unwanted" AE events can be used for tomographic imaging, too. Moreover, structural elements and acoustically "passive" defects can also be visualised. Finally, also AE events artificially generated, e.g. by pencil lead breaks or hammer impacts at outer surfaces of the specimen can be used for tomographic imaging. Thus, it seems that in many cases traditional

acoustic tomography with fixed and inflexible ray coverage could be replaced by adaptive AE tomography where tomographic inversion takes place on a ray-by-ray or rather an event-by-event basis. Based on the previous iteration the investigator could interactively decide if and where a higher resolution of the tomographic image is necessary and consequently, where the next AE event should be placed manually.

As has been shown in the discussion of the tomographic images in Figs. 6 and 7, there is still a lot of room for improvements of the underlying algorithms. Varieties of algebraic reconstruction techniques using curved ray paths should be tested for applicability in AE tomography in the future. Also the development of transform based tomography algorithms similar to the filtered backprojection algorithm seems to be worthwhile. Moreover, since in nondestructive evaluation strong scatterers are typical, the development of algorithms for AE reflection tomography (e.g. filtered backpropagation or synthetic aperture focusing technique, SAFT [7]) should be considered.

So far, the physical soundness of acoustic emission tomography has been shown by idealised numerical data only. In the future, more realistic models including heterogeneity of the concrete matrix and more complicated crack mechanisms will be investigated. Real measurements at concrete beams (using pencil lead breaks as AE sources) and aluminum plates (using Lamb waves for tomography) are under way in order to verify AE tomography experimentally. Based on the results obtained so far it can be expected that acoustic emission tomography has great potential for future applications offering totally new perspectives for acoustic emission imaging and acoustic tomography in general.

References

[1] Kak, A.C., and Slaney, M., *Principles of Computerized Tomographic Imaging*, IEEE Press, New York, 1988.

[2] Schechter, R.S., Mignogna, R.B., and Delsanto, P.P., "Ultrasonic tomography using curved ray paths obtained by wave propagation simulations on a massively parallel computer", J. Acoust. Soc. Am. **100** (4), 2103-2111, 1996.

[3] Mignogna, R.B., and Delsanto, P.P., "A parallel approach to acoustic tomography", J. Acoust. Soc. Am. **99** (4), 2142-2147, 1996.

[4] Fellinger, P., Marklein, R., Langenberg, K. J., and Klaholz, S., "Numerical modelling of elastic wave propagation and scattering with EFIT – Elastodynamic finite integration technique", Wave Motion **21**, 47-66, 1995.

[5] Schubert, F., and Schechinger, B., "Numerical modelling of acoustic emission sources and wave propagation in concrete", NDTnet, the e-Journal of Nondestructive Testing, Vol. **7**, No. 9, 2002 (http://www.ndt.net/article/v07n09/07/07.htm).

[6] Reinhardt, H.W., and Grosse, C.U., "Continuous monitoring of setting and hardening of mortar and concrete", Construction and Building Materials **18**, 145-154, 2004.

[7] Langenberg, K.J., Berger, M., Kreutter, T., Mayer, K., and Schmitz, V., "Synthetic aperture focusing technique signal processing", NDT International, Vol. **19**, No. 3, 177-189, 1986.